RSC Advances

ROYAL SOCIETY OF CHEMISTRY

PAPER

View Article Online
View Journal | View Issue

Cite this: *RSC Adv.*, 2025, **15**, 16337

Green synthesis and adsorption performance of Fe_3O_4/chitosan/polypyrrole composites for efficient removal of chromium ion†

Le Yin, Kai Wang, Liping Jiang, Yang Xi, Ziyi Xu, Zewen Song and Haijun Zhou *

Received 6th February 2025
Accepted 7th April 2025

DOI: 10.1039/d5ra00872g

rsc.li/rsc-advances

In this study, Fe_3O_4/chitosan/polypyrrole (Fe_3O_4/CS/PPy) magnetic adsorbents were successfully synthesized using the *in situ* chemical oxidation polymerization method. These adsorbents were characterized by SEM, FT-IR, TGA, and XPS. The results of batch adsorption experiments showed that the Fe_3O_4/CS/PPy composite exhibited a maximum adsorption capacity of 193.23 mg g^{-1} in a 100 mg L^{-1} Cr(VI) solution at 298 K, with a pH of 2.0. The adsorption behavior of the adsorbent to Cr(VI) was in good agreement with the Langmuir isothermal model and the quasi-second-order kinetic model. Thermodynamic studies indicated that the process of adsorption was spontaneous and endothermic. The mechanism of adsorption may be attributed to electrostatic interactions and chemical reduction. After five cycles, the removal efficiency of the Fe_3O_4/CS/PPy composite for Cr(VI) has consistently remained at 84.32%. Overall, the Fe_3O_4/CS/PPy composite exhibits great potential as an adsorbent for effectively removing Cr(VI) from aqueous solutions.

1. Introduction

Chromium-containing compounds are an important class of chemical raw materials.[1] The rapid development of industry has led to the significant emission of large amounts of Cr(VI) into the environment. Cr(VI) can become concentrated in water, atmosphere, and soil, and it can migrate through thermodynamic or kinetic mechanisms and eventually bioaccumulate in organisms. Therefore, Cr(VI) is a hazardous substance that significantly threatens the environment and sustainable human development.[2] Chromium typically occurs in two forms: Cr(III) (as Cr_2O_3 and $Cr(OH)_3$) and Cr(VI) (as $HCrO_4^-$, CrO_4^{2-} and $Cr_2O_7^{2-}$). The toxicity of Cr(VI) is significantly greater than that of Cr(III). Due to the oxidation of Cr(VI) and its high permeability to the skin, Cr(VI) is seriously harmful to the human respiratory tract, digestive tract, and skin mucosa.[3] Cr(VI) has been identified as a carcinogen with significant carcinogenic effects by the International Agency for Research on Cancer and the American Toxicology Organization. The World Health Organization has established maximum permissible limits for Cr(VI) in industrial wastewater and domestic water at 0.25 mg L^{-1} and 0.05 mg L^{-1}, respectively.[4] Therefore, there is an urgent need to develop efficient, expeditious, and effective approaches to alleviate Cr(VI) pollution. Among the various methods available for the removal of Cr(VI), such as chemical precipitation, membrane separation, ion exchange, and adsorption,[5,6] the latter has gained increasing attention in recent years due to its low cost, high removal efficiency, environmental friendliness, and ease of operation. Currently, a variety of adsorbents have been utilized for the removal of Cr(VI), such as biochar,[7] metal–organic skeletons,[8] zeolite,[9] clay minerals,[10] cellulose,[11] and diatomite.[12] However, the disadvantages of low adsorption capacity and high cost restrict the further utilization of adsorbents. Therefore, the development of low-cost, high-performance adsorbents is an urgent issue.

Polypyrrole (PPy) is a synthetic polymer that is rich in imino groups (–NH–) and possesses numerous advantages, including non-toxicity, low price, facile synthesis, and high chemical stability.[13] The chain of PPy contains nitrogen atoms with positive charges, which enables it to bind with Cr(VI) anions and effectively reduce them to Cr(III).[14] Although PPy is an effective absorbent material for the removal of Cr(VI), its small particle size makes it prone to loss in water, leading to potential secondary pollution. Additionally, PPy usually requires combining with different carriers to improve its processability and separability.[15] It is noteworthy that magnetic separation technology has found extensive applications in the field of adsorption.[16,17] The rapid separation and convenient recycling of the adsorbent can be easily achieved through an external magnetic field. It is worth noting that PPy particles tend to self-aggregate due to the strong π–π interaction between PPy molecular chains, which poses another significant issue. This ultimately results in a decrease in their specific surface area, leading to inadequate mass transfer performance. Chitosan (CS) is an inexpensive, non-toxic, and biodegradable natural

School of Materials Science and Engineering, Jiangsu University of Science and Technology, Zhenjiang, 212100, China. E-mail: zhouhaijun@just.edu.cn

† Electronic supplementary information (ESI) available. See DOI: https://doi.org/10.1039/d5ra00872g

adsorbent.[18] Owing to the abundance of amino ($-NH_2$) and hydroxyl (–OH) functional groups in its molecular structure, chitosan can form chelates with metal ions and is widely utilized for the removal of heavy metal ions from wastewater.[19,20] Although CS readily dissolves in acidic environments, it is conducive to the growth of PPy, which helps to irregular aggregation of PPy through hydrogen bonds. Shi *et al.* prepared an EDTA-CS/PPy composite with multiple abundant types of adsorption sites, thereby achieving the simultaneous removal of Cr(VI) anions and other metal cations.[21]

In this study, the Fe_3O_4/CS/PPy composites were synthesized using a one-pot synthesis method. Firstly, Fe_3O_4 nanoparticles were synthesized *via* a hydrothermal approach. The superparamagnetic properties of Fe_3O_4 ensured convenient recycling after adsorption. Then, PPy was synthesized by chemical oxidative polymerization, and finally, the composite was formed by simple physical blending. The preparation process was conducted in an environmentally friendly manner, without the incorporation of a cross-linking agent. The adsorbents were characterized through SEM, FT-IR, TGA, and XPS. The effects of pH, initial concentration of Cr(VI), and dosage of adsorbents on the adsorption performance were investigated. To elucidate the adsorption mechanism of adsorbent, the adsorption kinetics, isotherms, and thermodynamics experiments were conducted. Furthermore, regeneration and recyclability experiments were also conducted to evaluate the potentiality of this novel adsorbent.

2. Material and methods

2.1. Chemicals and materials

Potassium dichromate ($K_2Cr_2O_7$), trisodium citrate dihydrate ($Na_3C_6H_5O_7 \cdot 2H_2O$), iron chloride hexahydrate ($FeCl_3 \cdot 6H_2O$), ethylene glycol(EG), sodium acetate anhydrous (CH_3COONa), chitosan (CS), dilute hydrochloric acid (HCl), acetic acid, sodium hydroxide (NaOH), pyrrole (Py) and ammonium persulfate (APS) were purchased from Sinopharm Chemical Reagent Co., Ltd. All reagents used in this study were analytical grade, and the experimental water was prepared with deionized water.

2.2 Adsorbent preparation

2.2.1. Preparation of Fe_3O_4. Fe_3O_4 was synthesized using a hydrothermal method as follows.[22] 1.35 g of $FeCl_3 \cdot 6H_2O$ and 0.58 g of trisodium citrate dihydrate were mixed in 50 mL of ethylene glycol and stirred magnetically at 80 °C until a homogeneous mixture was achieved. Next, 3.0 g of sodium acetate anhydrous was added and stirred for 2 h. Then, the resulting mixture was transferred to a hydrothermal reactor at 200 °C for 12 h. Finally, the black precipitate was collected using a magnetic block and washed repeatedly with anhydrous ethanol and deionized water. Subsequently, the black powder was dried under a vacuum at 60 °C for 6 h.

2.2.2. Preparation of Fe_3O_4/CS/PPy. Briefly, 0.75 g of CS was dissolved in 20 mL of 1% (m/v) acetic acid solution. Then, 0.38 g of obtained Fe_3O_4 was ultrasonically dispersed in the CS solution, recorded as solution A. An additional 1% (m/v) acetic acid solution was introduced into a three-necked flask and subjected to an ice-water bath to maintain it at 2–5 °C. Subsequently, 3.0 g of pyrrole was added to the cryogenic solution and thoroughly stirred until a homogeneous solution was formed. Next, solution A was slowly added dropwise and stirred for 30 minutes to form a homogeneous mixture. Finally, 10.2 g of ammonium persulfate was added to the mixture and stirred continuously for 12 h in an ice bath. The product was magnetically separated and subsequently washed repeatedly with deionized water and anhydrous ethanol. Then, it was dried under a vacuum for 6 h at 60 °C. The synthesis route of the Fe_3O_4/CS/PPy composite is illustrated in Fig. 1.

2.3. Characterization

The scanning electron microscope (SEM) images were obtained using a Zeiss Merlin Compact field emission with an accelerating voltage of 20 kV. Fourier Transform infrared (FT-IR) spectra were obtained using the Bruker Equinox 55 spectrometer in transmission mode, and the scan range was from 4000 to 500 cm^{-1}. Thermogravimetric analysis (TGA) was performed with a Pyris Diamond thermogravimetric analyzer (PerkinElmer, USA) at a heating rate of 10 °C min^{-1} under a nitrogen atmosphere from room temperature to 800 °C. The charged properties of the surface of microspheres in different pH

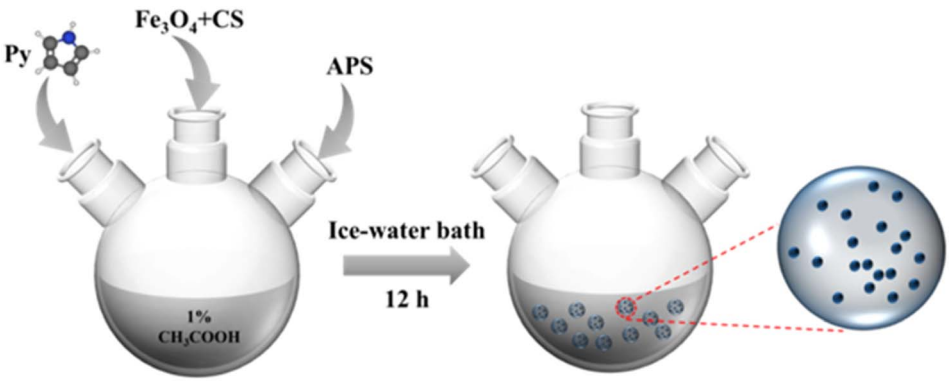

Fig. 1 The synthesis route of the Fe_3O_4/CS/PPy.

solutions can be analyzed by zeta (ζ) potentials. The instrument used is a Nanobrook 90Plus Zeta nano grain-sized analyzer (Brookhaven, USA), which is used at normal atmospheric temperature (25 °C). The X-ray photoelectron spectra (XPS) experiments were conducted using a PHI5800 X-ray photoelectron spectroscopy analyzer (ULVCA-PHI, USA). A UV-Vis spectrophotometer (UV-2550, Hitachi, Japan) was employed to conduct colorimetric measurements of Cr(VI) concentration.

2.4. Adsorption experiments

A typical adsorption experiment was conducted by adding the adsorbent to a 50 mL $K_2Cr_2O_7$ solution at various concentrations and pH values. To ensure the complete elimination of Cr(VI), the solution was continuously oscillated for 12 h at the designated temperature. Upon the completion of the experiment, an external magnet was utilized to collect the adsorbent. Using a UV-vis spectrophotometer, the chromium content in the solution was identified. Eqn. (1) and (2) were utilized to calculate the adsorption capacity of Cr(VI) at equilibrium conditions and at t time. The removal rate (R) of Cr(VI) ions was calculated using eqn (3)

$$Q_e = \frac{(C_0 - C_e)V}{m} \quad (1)$$

$$Q_t = \frac{(C_0 - C_t)V}{m} \quad (2)$$

$$R = \frac{(C_0 - C_e)}{C_0} \times 100\% \quad (3)$$

where C_0 and C_e (mg L^{-1}) represent respectively the initial and equilibrium concentration of Cr(VI) solution, C_t (mg L^{-1}) represents the concentration of Cr(VI) solution at t time, V (L) is the volume of the Cr(VI) solution, m (g) is the mass of adsorbent, Q_e and Q_t (mg g^{-1}) is the adsorption capacity at equilibrium conditions and at t time.

Effect of pH: a series of Cr(VI) solutions with a concentration of 100 mg L^{-1} at varying pH (2, 3, 4, 5, 6, 7, 8) were prepared by adding 0.1 M HCl or 0.1 M NaOH solution. Subsequently, an adsorbent dosage of 0.5 g L^{-1} was added to each flask, and the adsorption process was carried out at room temperature for 12 h.

Effect of adsorbent dosage: a series of Cr(VI) solutions with a concentration of 100 mg L^{-1} were prepared, and various dosages of adsorbent (0.1, 0.2, 0.3, 0.4, 05, 0.6, and 0.7 g L^{-1}) were added to the Cr(VI) solution. The adsorption was carried out at room temperature for 12 h, and the pH of the solution was 5.

Effect of the initial concentration of Cr(VI): a series of Cr(VI) solutions at varying concentrations (25 mg L^{-1}, 50 mg L^{-1}, 75 mg L^{-1}, 100 mg L^{-1}, 125 mg L^{-1}, 150 mg L^{-1}, and 175 mg L^{-1}) were prepared, the adsorbent was introduced into the Cr solution at a dosage of 0.5 g L^{-1}. The adsorption was carried out at room temperature for 12 h, and the pH of the solution was 5.

2.5. Adsorption kinetics

The adsorption kinetic curve illustrates the rate of adsorption of Cr(VI) on the surface of the adsorbent and the corresponding amount of adsorption *versus* time.

The adsorption kinetics and mechanism were investigated using the quasi-first-order kinetic models, quasi-second-order kinetic models, and intraparticle diffusion models. The initial concentrations of Cr(VI) solutions were 50 mg L^{-1}, 100 mg L^{-1}, and 150 mg L^{-1}, respectively. An adsorbent dosage of 0.5 g L^{-1} was added to the Cr(VI) solution. The adsorption experiments were carried out under controlled conditions of temperature (298 K), initial pH (5), and adsorption time (10 h). The concentration of Cr(VI) remaining in the solution was measured at specific intervals.

2.6. Adsorption isotherms and thermodynamics

Adsorption isotherms describe the interaction mechanism between the adsorbent and adsorbate and can be used to evaluate the adsorbent's adsorption capacity. Thermodynamic studies help to understand whether the adsorption behavior is absorptive or exothermic. Several experiments were conducted at different temperatures (298 K, 308 K, 318 K, and 328 K) using varying concentrations of Cr(VI) solutions (ranging from 50 to 500 mg L^{-1} with an interval of 50 mg L^{-1}) at a pH of 5. A concentration of 0.5 g L^{-1} of adsorbent was added to the solution containing Cr(VI) and shaken for 10 h.

2.7. Regeneration of the sorbent elution

To desorb the adsorbed Cr(VI), the adsorbent after adsorption was immersed in 25 mL of 0.1 M NaOH for 6 h. Subsequently, the adsorbent was retrieved using a magnet, thoroughly washed with deionized water and anhydrous ethanol, and then dried under a vacuum at 60 °C for 6 h. The regenerated pellets were subjected to 5 adsorption and desorption cycles under identical conditions. The adsorption experiments were carried out at a temperature of 298 K, an initial pH of 5, an initial concentration of Cr(VI) of 100 mg L^{-1}, and an adsorption time of 12 h.

3. Results and discussions

3.1. Characterization of Fe_3O_4/CS/PPy

3.1.1. SEM. The SEM images of Fe_3O_4, Fe_3O_4/CS, and Fe_3O_4/CS/PPy composites are presented in Fig. 2. From the SEM images, it can be seen that the morphology of the composites was spherical and uniformly dispersed. The average particle sizes of Fe_3O_4/CS/PPy were found to be less than 100 μm. The surface of Fe_3O_4/CS/PPy became smoother due to the deposition of a polypyrrole coating layer on the surface of the Fe_3O_4/CS microspheres. The microsphere structure possesses a large specific surface area, thereby enhancing its adsorption capacity for Cr(VI).

3.1.2. FT-IR spectra. The FT-IR spectra of CS and Fe_3O_4/CS/PPy are presented in Fig. 3. In the Fe_3O_4/CS/PPy composite, the peak observed at 583 cm^{-1} corresponds to the stretching vibration of Fe–O.[23] The peaks at 1485 cm^{-1}, 1299 cm^{-1}, 1113 cm^{-1}, 890 cm^{-1}, and 780 cm^{-1} are characteristic peaks of PPy,[24] indicating that the product contains PPy. The absorption peak between 3225 cm^{-1} and 3639 cm^{-1} is attributed to the overlapping stretching vibrations of –NH– and –OH. The peaks at 1304 cm^{-1} and 703 cm^{-1} are attributed to the O–H bending

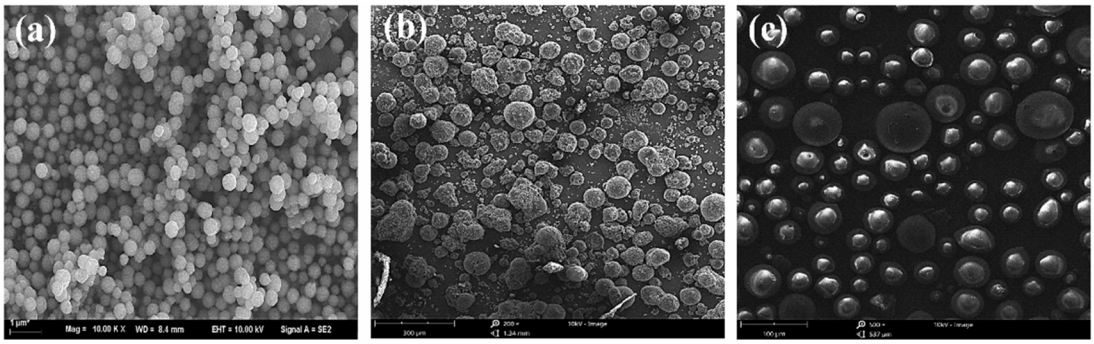

Fig. 2 The SEM images of (a) Fe_3O_4, (b) Fe_3O_4/CS, (c) Fe_3O_4/CS/PPy.

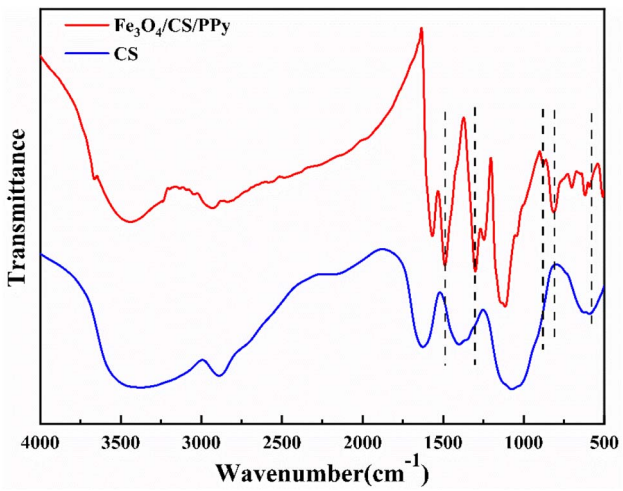

Fig. 3 FT-IR spectra of CS and Fe_3O_4/CS/PPy.

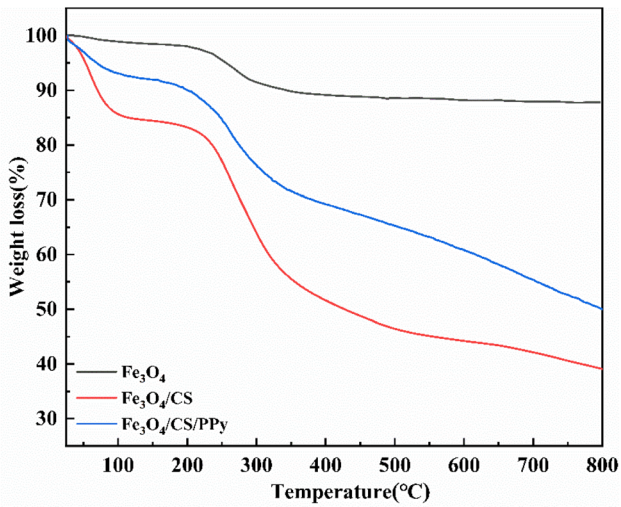

Fig. 4 TG curves of Fe_3O_4, Fe_3O_4/CS, and Fe_3O_4/CS/PPy composite.

vibrations of CS molecules inside and outside, respectively. The peak at 1123 cm^{-1} corresponds to the C–O–C stretching vibration of the molecular chain in CS.[25] The stretching vibration of C=O at 1649 cm^{-1} in CS disappeared. However, a new peak at 1565 cm^{-1} appeared due to the electrostatic interaction between the $-NH_2$ group of CS and the π-electron system of PPy. The results presented above demonstrate the successful preparation of the Fe_3O_4/CS/PPy composite.

3.1.3. TGA. The thermogravimetric curves of Fe_3O_4, Fe_3O_4/CS, and Fe_3O_4/CS/PPy composite were recorded in Fig. 4. The thermal decomposition of Fe_3O_4 consists of two stages, and the thermal decomposition of Fe_3O_4/CS and Fe_3O_4/CS/PPy consists of three phases.[26] As the temperature increased from 25 to 200 °C, the weight loss of Fe_3O_4, Fe_3O_4/CS, and Fe_3O_4/CS/PPy composites was attributed to the evaporation of the adsorbed water in the samples. The weight loss platform of Fe_3O_4 was observed at 200 °C, which can be attributed to the decomposition of the residual organic groups during the preparation process of Fe_3O_4. The weight of the Fe_3O_4 remained relatively stable at 800 °C, exhibiting good thermal stability. The TG curve of Fe_3O_4/CS and Fe_3O_4/CS/PPy composites exhibited distinct differences from that of pure Fe_3O_4, which can be attributed to the incorporation of CS and PPy. With the increase in temperature, rapid weight loss occurs when the temperature exceeds 350 °C, mainly due to the carbonization and degradation of CS and PPy.

3.2. Adsorption studies

3.2.1. Effect of adsorbent dosage. The amount of adsorbent utilized for the removal of metal ions plays a critical role in attaining equilibrium between the sorbent and sorbate species. The adsorption capacity of Fe_3O_4/CS/PPy exceeds that of Fe_3O_4, CS, and Fe_3O_4/CS (Fig. S1†). As illustrated in Fig. 5(a), the adsorption capacity of the Fe_3O_4/CS/PPy composite for Cr(VI) decreased from 142.16 mg g^{-1} to 113.08 mg g^{-1} as the adsorbent dosage increased. This is likely because many active sites were obscured with the increase in adsorbent dosage. The number of adsorption sites exceeded the amount of Cr(VI) in solution when Fe_3O_4/CS/PPy was added in excess, and Cr(VI) was unable to fully occupy all the adsorption sites of Fe_3O_4/CS/PPy.[27] In other words, the adsorption capacity (Q_e) demonstrated a significant reduction, which can be attributed to the direct proportionality of Q_e to ($C_0 - C_e$) and inverse proportionality to the mass of the adsorbent.

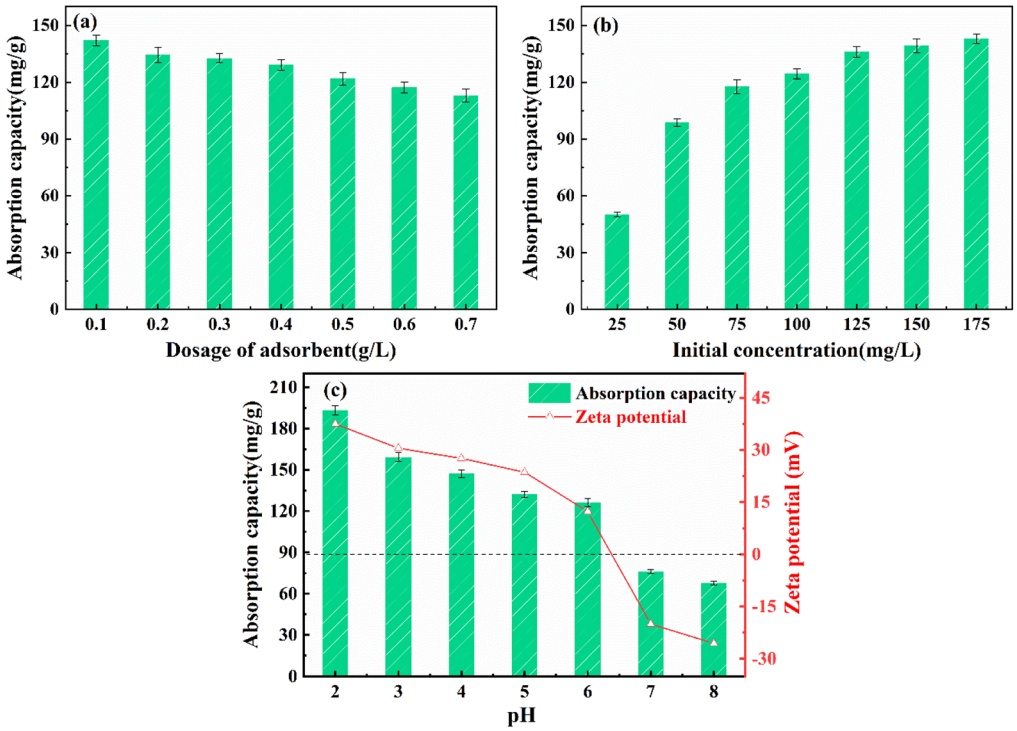

Fig. 5 Effect of the preparation conditions on adsorption capacity. (a) Fe_3O_4/CS/PPy dosage (pH = 5, solution concentration = 100 mg L^{-1}), (b) initial concentration of Cr(VI) (pH = 5, adsorbent dose = 25g L^{-1}), (c) pH value (solution concentration = 100 mg L^{-1}, adsorbent dose = 25g L^{-1}). All contact time = 720 min, T = 298 K.

3.2.2. Effect of initial Cr(VI) concentration. The effect of the initial concentrations of Cr(VI) on the adsorption capacity is shown in Fig. 5(b). The adsorption capacity of Fe_3O_4/CS/PPy composite increased from 50.0 mg g^{-1} to 142.96 mg g^{-1} as the initial concentration of Cr(VI) increased from 25 mg L^{-1} to 175 mg L^{-1}. This can be attributed to the fact that at a lower concentration of Cr(VI), the number of adsorption sites on the surface of the Fe_3O_4/CS/PPy composite was significantly higher than the amount of Cr(VI) present in the solution. As the initial concentration of Cr(VI) increased, more adsorption sites were occupied by Cr(VI), gradually increasing adsorption capacity. However, increasing the initial concentration of Cr(VI) would fully occupy the adsorption active sites on Fe_3O_4/CS/PPy. As a result, adsorption equilibrium would be reached due to spatial site resistance.[28]

3.2.3. Effect of pH value. The pH value of a solution is a crucial factor that significantly impacts the adsorption of heavy metal ions. This is due to the close relationship between the morphology of heavy metal ions and the pH value of the solution. The Fe_3O_4/CS/PPy exhibited good stability in the different pH solutions (Fig. S2†). Fig. 5(c) illustrates the effect of pH value on the adsorption capacity. The adsorption capacity gradually decreased as the pH increased from 2 to 8. The optimal adsorption capacity (193.23 mg g^{-1}) was observed at an initial pH value of 2. The adsorption capacity decreased from 126.20 mg g^{-1} to 76.20 mg g^{-1} as the pH increased from 6 to 7. This observation may be attributed to the speciation of chromium ions in the solution. When the pH value is below 7, Cr(VI) primarily exists in the forms of $HCrO_4^-$ and $Cr_2O_7^{2-}$. The Fe_3O_4/CS/PPy complex exhibited an increased affinity for Cr(VI) due to the presence of –NH_2 and –OH on its surface.[29] When the pH value exceeds 7, Cr(VI) primarily exists in the form of $Cr_2O_7^{2-}$ and CrO_4^{2-}. In this case, OH^- ions in the solution compete with Cr(VI) for adsorption sites on the surface of the adsorbent. Thus, the adsorption capacity for Cr(VI) decreased under alkaline conditions.

3.3. Adsorption kinetics

The kinetic data were analyzed using a quasi-first-order kinetic model, a quasi-second-order kinetic model, and an intraparticle diffusion kinetic model to provide an interpretation. Fig. 6(a) illustrates the adsorption kinetics of Cr(VI) on the Fe_3O_4/CS/PPy composite at 25 °C. The adsorption capacity increased with an increase in the concentration of Cr(VI). Within 60 minutes of adsorption, the adsorption rate was relatively fast. As the adsorption time increased, the adsorption rate gradually decreased and eventually reached equilibrium. The initial rapid adsorption rate can be attributed to the presence of an adequate number of unoccupied adsorption sites. As the adsorption time was prolonged, the active sites for adsorption gradually became occupied, leading to a reduction in the concentration of free Cr(VI) in the solution. Consequently, the adsorption rate of Cr(VI) was relatively low. Equilibrium was reached after 330 minutes of adsorption. The corresponding equilibrium adsorption capacities were 254.45 mg g^{-1}, 299.40 mg g^{-1}, and 369.00 mg g^{-1} for initial Cr(VI) concentrations of 50 mg L^{-1}, 100 mg L^{-1}, and 150 mg L^{-1}, respectively.

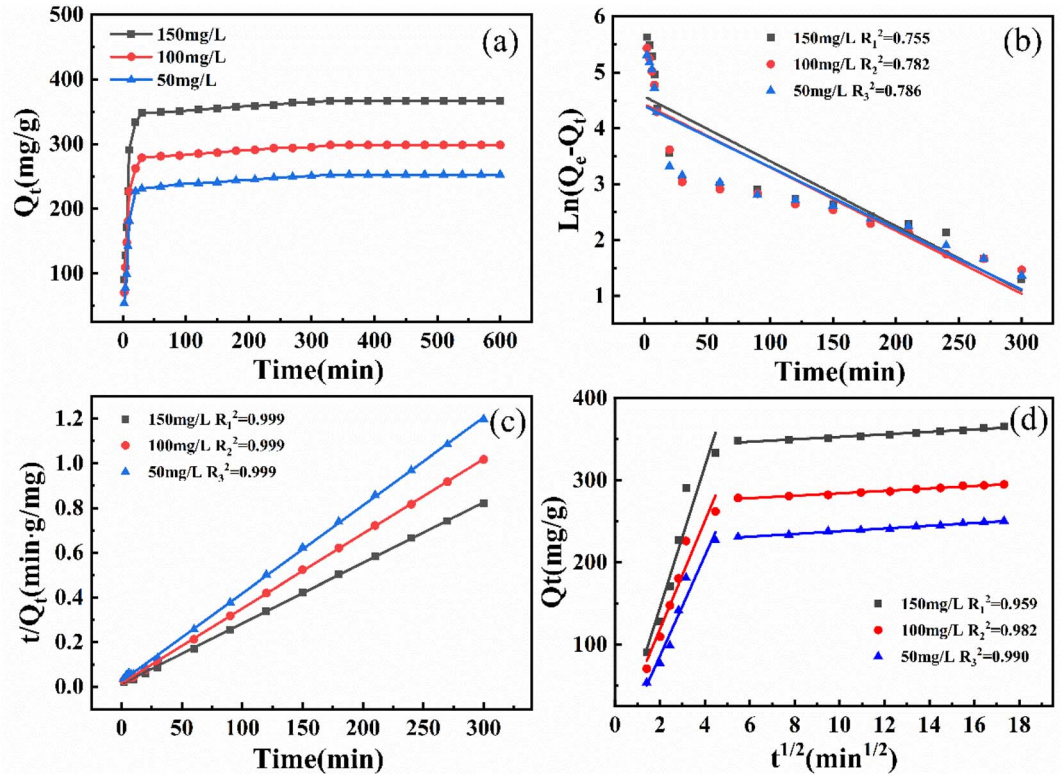

Fig. 6 (a) The effects of adsorption time on the adsorption capacity of Cr(VI) at different concentrations, (b) quasi-first-order kinetics, (c) quasi-second-order kinetics, and (d) intraparticle diffusion kinetics.

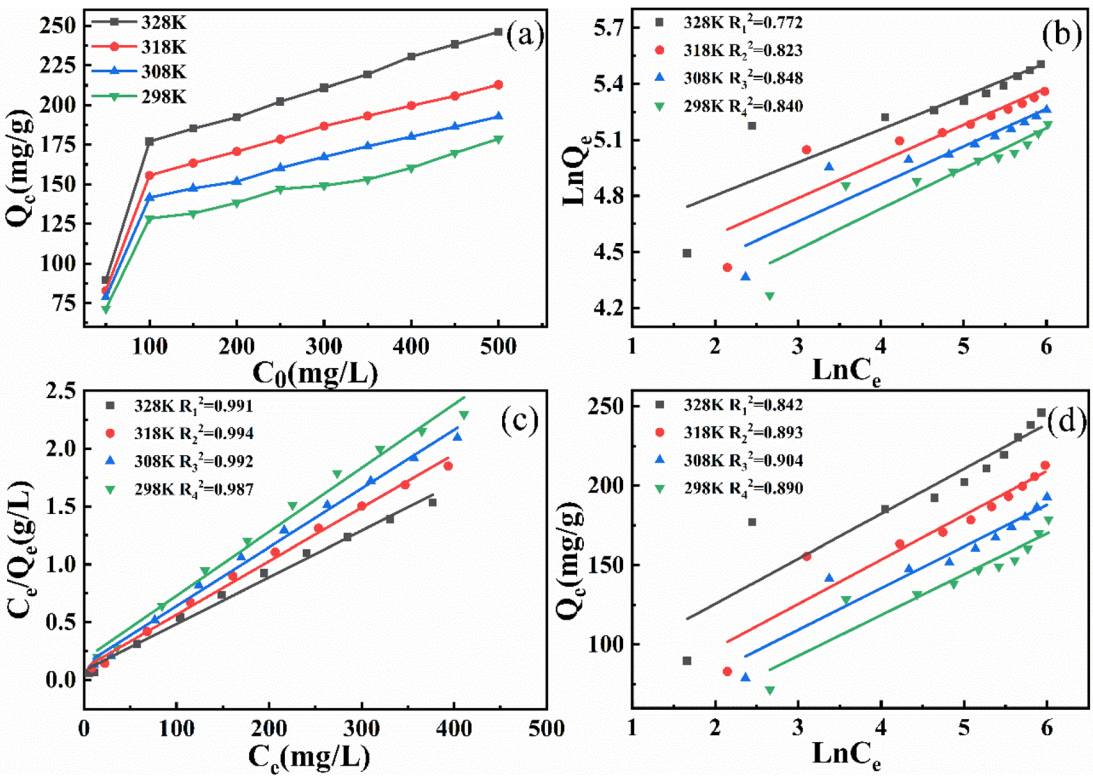

Fig. 7 (a) Adsorption isotherm, (b) Freundlich isotherm model, (c) Langmuir isotherm model and (d) Temkin isotherm model.

Table S1† presents the statistical analysis results regarding the validity of the selected kinetic models. Fig. 6(b) illustrates a linear deviation observed in the quasi-first-order model. This could be attributed to the strong adsorption during the initial adsorption phase. Based on the results, it can be concluded that the fitted quasi-second-order curve (Fig. 6(c)) is the most appropriate fit, as all data points exhibit an R^2 value greater than 0.99. Furthermore, the experimental data and simulated quantitative values showed a high degree of concurrence, suggesting that chemisorption plays a pivotal role in controlling the rate of the process. As a result, the primary adsorption mechanism of Cr(VI) by Fe_3O_4/CS/PPy was governed by chemical adsorption.[30]

The intraparticle diffusion model is utilized to elucidate the rate-controlling steps of the adsorption process (Fig. 6(d)). A comparable adsorption pattern was observed when Fe_3O_4/CS/PPy was treated with Cr(VI) solutions of varying initial concentrations. The higher the value of C, the more significant the influence of surface adsorption on the rate-controlling mechanism. The C value increases with the initial concentration of Cr(VI), suggesting that at higher concentrations, the binding layer has a more pronounced effect on the adsorption of Cr(VI). Q_t and $t^{1/2}$ are linear, and lines do not pass through the origin, which indicates that in addition to intra-particle diffusion, the adsorption process also received the influence of boundary layer diffusion. As the concentration of Cr(VI) increases, the number of adsorption sites occupied by Cr(VI) gradually increases, leading to the thickening of the boundary layer on the adsorbent surface. The thicker boundary layer impeded the diffusion of Cr(VI) from the solution to the absorbent, resulting in a slower diffusion rate.[31]

3.4. Adsorption isotherms and thermodynamics

Fig. 7(a) demonstrates the effects of temperature variation on the adsorption capacity of Fe_3O_4/CS/PPy for Cr(VI). The adsorption capacity for Cr(VI) increased rapidly when the initial concentration was low and then increased slowly over an extended concentration range. This may be because as the concentration of Cr(VI) increased, the chances of Cr(VI) binding to the adsorption sites increased. In addition, at the same concentration, molecular motion accelerates with increasing temperature, and the adsorption capacity for Cr(VI) increases. To fit the adsorption isotherms of the adsorbent on Cr(VI), the Freundlich model, the Langmuir model, and the Temkin isotherm model were used (Fig. 7(b–d)). The fitted isotherm parameters are as shown in Table S2.† The R^2 value of the Langmuir isotherm model is higher than that of the Freundlich and Temkin isotherm models, indicating a better fit of the Langmuir model to the experimental data. Therefore, the adsorption process conforms more closely to the Langmuir model, suggesting that monolayer adsorption is the dominant mechanism.[32]

Calculated thermodynamic parameters for Cr(VI) adsorption on Fe_3O_4/CS/PPy are listed in Table S3.† From the Van't Hoff plot (Fig. S3†), it can be seen that the correlation coefficient is 0.963, indicating a good fit for the data. Furthermore, since ΔH (10.68 kJ mol^{-1}) > 0, the adsorption process can be characterized as an exothermic reaction. The positive ΔS value of 33.88 J (mol^{-1} K^{-1}) suggests that the primary mechanism promoting the adsorption of Cr(VI) is an entropic effect. This indicates that the adsorption of Cr(VI) results in greater stability and randomness at the solid–solution interface, which leads to an increase in entropy.[33] As the temperature increased from 298 to 328 K, the ΔG value decreased from −0.31 to −1.42 kJ mol^{-1}. Increasing the temperature facilitates the adsorption process. Therefore, this result is consistent with the adsorption isotherm and kinetics. In summary, the positive values of ΔH, ΔS, the negative value of ΔG indicate that the adsorption of Cr(VI) on Fe_3O_4/CS/PPy is a favorable and spontaneous process.[34]

3.5. Regeneration

The regenerative performance of adsorbent materials is an important factor in determining their actual applicability. The regeneration process of Fe_3O_4/CS/PPy composite was carried out using 0.1 M NaOH as the eluent. Fig. 8 shows the removal

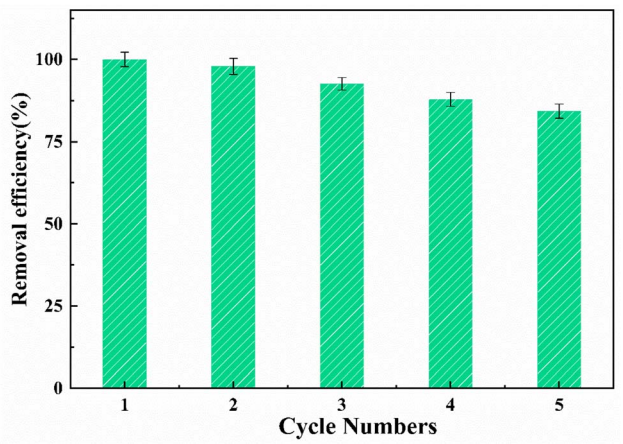

Fig. 8 Removal efficiency of Fe_3O_4/CS/PPy composite in five cycles of regeneration experiment. (Solution concentration = 100 mg L^{-1}, pH = 5, adsorbent dose = 25g L^{-1}, T = 298 K, contact time = 720 min).

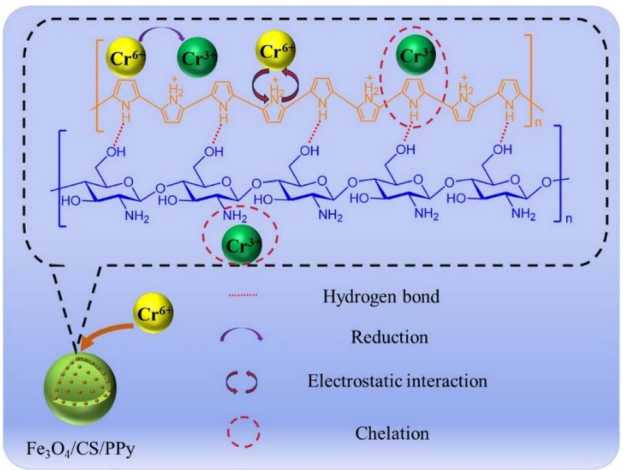

Fig. 9 Adsorption mechanism of Fe_3O_4/CS/PPy composites.

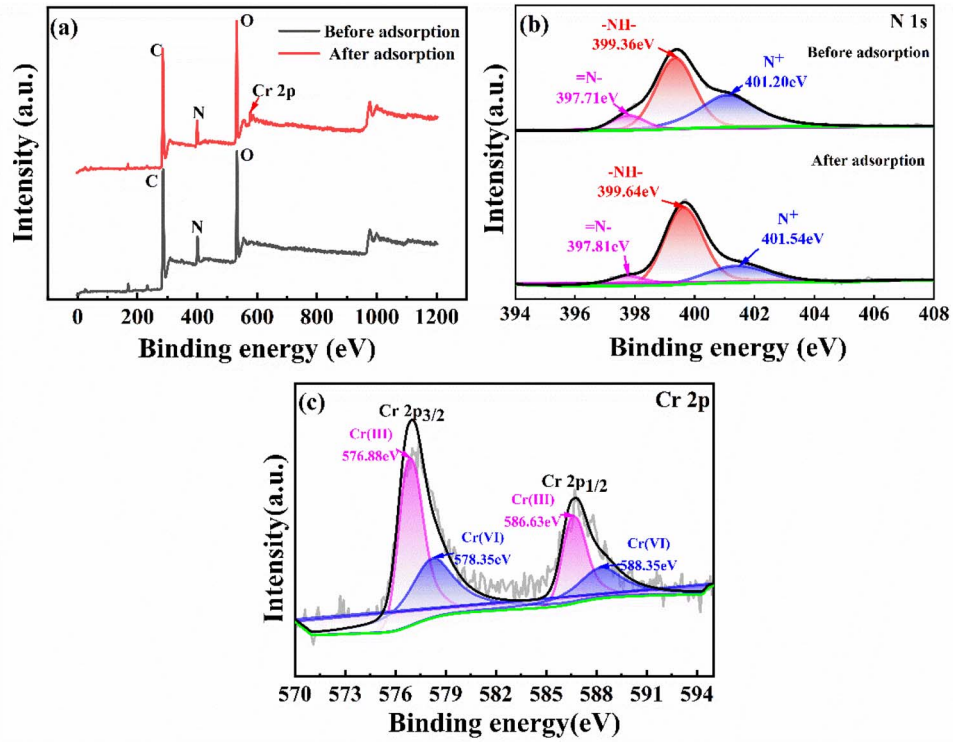

Fig. 10 (a) XPS full spectrum of Fe_3O_4/CS/PPy before and after Cr(VI) adsorption. (b) N 1s spectrum before and after adsorption. (c) Cr 2p spectrum after adsorption.

efficiency of Fe_3O_4/CS/PPy composite throughout 5 cycles. The removal efficiency of Fe_3O_4/CS/PPy composite material decreased slightly, with only about a 12% decrease observed in cycles 1–4, but still maintained a removal efficiency of 84.34% after the fifth cycle. As the desorption process was conducted under alkaline conditions, a minor loss of adsorbent may occur during the adsorption–desorption cycle process. Some of the adsorption sites on the surface were not completely desorbed by NaOH and remained occupied by the previous Cr(VI) ions.[35] The results indicated that the Fe_3O_4/CS/PPy composites exhibited good stability and regeneration performance.

3.6. Adsorption mechanisms

The adsorption mechanism of Fe_3O_4/CS/PPy composites on Cr(VI) is illustrated in Fig. 9. To assess the adsorption mechanism of Fe_3O_4/CS/PPy composites for Cr(VI), XPS analysis was performed on Fe_3O_4/CS/PPy composites prior and after adsorption, respectively. As shown in Fig. 10(a), the Fe_3O_4/CS/PPy composites exhibited a new characteristic peak after adsorption, corresponding to the Cr energy band, indicating that Cr(VI) was adsorbed on the materials. In Fig. 10(c), the energy bands of Cr 2 $p_{3/2}$ and Cr 2 $p_{1/2}$ are 575–579 eV and 585–589 eV, respectively, which indicates the presence of Cr(III) and Cr(VI) in the Fe_3O_4/CS/PPy composites.[36] In an acidic medium, Cr(VI) exhibits a higher oxidation potential, facilitating its easy reduction to less toxic Cr(III) by the electron-rich PPy present in the adsorbent material. Consequently, a portion of absorbed Cr(VI) was reduced to Cr(III).[37] The possible reactions may occur according to eqn. (4) and (5).[38]

$$Cr_2O_7^{2-} + 6PPy^0/CS/Fe_3O_4 + 14H^+ \rightarrow 2Cr^{3+} + 6PPy^+/CS/Fe_3O_4 + 7H_2O \quad (4)$$

$$HCrO_4^- + 3PPy^0/CS/Fe_3O_4 + 7H^+ \rightarrow Cr^{3+} + 3PPy^+/CS/Fe_3O_4 + 4H_2O \quad (5)$$

From the high-resolution XPS spectra of N 1s (Fig. 10(b)), it can be observed that the binding energies of $=NH^-$, –NH–, and N^+ in the adsorbed sample are increased. This suggests that the nitrogen atoms in PPy participated in the adsorption reaction. The adsorption process is mainly accomplished through electrostatic attraction between N^+ and Cr(VI) ($Cr_2O_7^{2-}$ and $HCrO_4^-$) as well as a redox reaction between Fe_3O_4/CS/PPy and Cr(VI). Moreover, the $-NH_2$ groups in the CS and the deprotonated pyrrolic N sites can adsorb Cr(III) through the formation of a covalent bond between Cr(III) and N, resulting in the formation of a complex that is immobilized on the adsorbent.[39,40]

4. Conclusions

Fe_3O_4/CS/PPy composites with abundant adsorption sites were prepared using simple blending and chemical oxidative polymerization, which was employed for Cr(VI) removal and exhibited excellent adsorption performance. The results indicated that Fe_3O_4/CS/PPy composites exhibited optimal

adsorption performance under pH 2, with a maximum adsorption capacity for Cr(VI) of 193.23 mg g^{-1} at 298 K. The adsorption process of Cr(VI) on the Fe_3O_4/CS/PPy composite conformed to a quasi-second-order kinetic model and the Langmuir model. The thermodynamic studies indicate that the adsorption is a spontaneous process. After several adsorption and regeneration cycles, the adsorbent maintained a high removal efficiency of Cr(VI). The results further suggested that electrostatic interaction, chelation, and redox reaction are the dominant adsorption mechanisms. According to the present study, Fe_3O_4/CS/PPy will be a reference for practical application to remove Cr(VI) from wastewater due to its green preparation process, low raw material cost, excellent adsorption, and recycling performance.

Data availability

The authors affirm that the data supporting the findings of this study are included in the article. Additional data can be made available from the corresponding author upon reasonable request.

Author contributions

Haijun Zhou: data curation, funding acquisition, project administration, supervision, writing – review & editing. Le Yin: data curation, formal analysis, methodology, writing – original draft. Kai Wang: data curation, formal analysis, writing – review & editing. Liping Jiang: data curation, investigation. Yang Xi: formal analysis, investigation. Ziyi Xu: investigation, methodology. Zewen Song: investigation, methodology.

Conflicts of interest

The authors declare that they have no known competing financial interests or personal relationships that could have appeared to influence the work reported in this paper.

Acknowledgements

This work was supported by Jiangsu University of Science and Technology.

References

1 J. J. Coetzee, N. Bansal and E. M. N. Chirwa, Chromium in Environment, Its toxic effect from chromite-mining and ferrochrome industries, and its possible bioremediation, *Exposure Health*, 2018, **12**(1), 51–62, DOI: **10.1007/s12403-018-0284-z**.

2 S. Prasad, K. K. Yadav, S. Kumar, N. Gupta, M. M. S. Cabral-Pinto, S. Rezania, N. Radwan and J. Alam, Chromium contamination and effect on environmental health and its remediation: A sustainable approaches, *J. Environ. Manage.*, 2021, **285**, 112174, DOI: **10.1016/j.jenvman.2021.112174**.

3 G. Genchi, G. Lauria, A. Catalano, A. Carocci and M. S. Sinicropi, The Double Face of Metals: The Intriguing Case of Chromium, *Appl. Sci.*, 2021, **11**(2), 638, DOI: **10.3390/app11020638**.

4 H. Demiral, İ. Demiral, F. Tümsek and B. Karabacakoğlu, Adsorption of chromium (VI) from aqueous solution by activated carbon derived from olive bagasse and applicability of different adsorption models, *Chem. Eng. J.*, 2008, **144**(2), 188–196, DOI: **10.1016/j.cej.2008.01.020**.

5 A. U. Rajapaksha, R. Selvasembian, A. Ashiq, V. Gunarathne, A. Ekanayake, V. O. Perera, H. Wijesekera, S. Mia, M. Ahmad, M. Vithanage and Y. S. Ok, A systematic review on adsorptive removal of hexavalent chromium from aqueous solutions: Recent advances, *Sci. Total Environ.*, 2022, **809**, 152055, DOI: **10.1016/j.scitotenv.2021.152055**.

6 H. Peng and J. Guo, Removal of chromium from wastewater by membrane filtration, chemical precipitation, ion exchange, adsorption electrocoagulation, electrochemical reduction, electrodialysis, electrodeionization, photocatalysis and nanotechnology: a review, *Environ. Chem. Lett.*, 2020, **18**(6), 2055–2068, DOI: **10.1007/s10311-020-01058-x**.

7 F. X. Dong, L. Yan, X. H. Zhou, S. T. Huang, J. Y. Liang, W. X. Zhang, Z. W. Guo, P. R. Guo, W. Qian, L. J. Kong, W. Chu and Z. H. Diao, Simultaneous adsorption of Cr (VI) and phenol by biochar-based iron oxide composites in water: Performance, kinetics and mechanism, *J. Hazard. Mater.*, 2021, **416**, 125930, DOI: **10.1016/j.jhazmat.2021.125930**.

8 J. Liu, Y. Ye, X. Sun, B. Liu, G. Li, Z. Liang and Y. Liu, A multifunctional Zr(VI)-based metal-organic-framework for highly efficient elimination of Cr(vi) from the aqueous phase, *J. Mater. Chem. A*, 2019, **7**(28), 16833–16841, DOI: **10.1039/c9ta04026a**.

9 M. R. Adam, N. M. Salleh, M. H. D. Othman, T. Matsuura, M. H. Ali, M. H. Puteh, A. F. Ismail, M. A. Rahman and J. Jaafar, The adsorptive removal of chromium (VI) in aqueous solution by novel natural zeolite based hollow fibre ceramic membrane, *J. Environ. Manage.*, 2018, **224**, 252–262, DOI: **10.1016/j.jenvman.2018.07.043**.

10 S. Gu, X. Kang, L. Wang, E. Lichtfouse and C. Wang, Clay mineral adsorbents for heavy metal removal from wastewater: a review, *Environ. Chem. Lett.*, 2018, **17**(2), 629–654, DOI: **10.1007/s10311-018-0813-9**.

11 Y. Wang, L. Yu, R. Wang, Y. Wang and X. Zhang, A novel cellulose hydrogel coating with nanoscale Fe^0 for Cr (VI) adsorption and reduction, *Sci. Total Environ.*, 2020, **726**, 138625, DOI: **10.1016/j.scitotenv.2020.138625**.

12 A. Hethnawi, W. Khderat, K. Hashlamoun, A. Kanan and N. N. Nassar, Enhancing chromium (VI) removal from synthetic and real tannery effluents by using diatomite-embedded nanopyroxene, *Chemosphere*, 2020, **252**, 126523, DOI: **10.1016/j.chemosphere.2020.126523**.

13 L. Xiang, C. G. Niu, N. Tang, X. X. Lv, H. Guo, Z. W. Li, H. Y. Liu, L. S. Lin, Y. Y. Yang and C. Liang, Polypyrrole coated molybdenum disulfide composites as adsorbent for enhanced removal of Cr (VI) in aqueous solutions by adsorption combined with reduction, *Chem. Eng. J.*, 2021, **408**, 127281, DOI: **10.1016/j.cej.2020.127281**.

14 P. Liang, S. Liu, M. Li, W. Xiong, X. Yao, T. Xing and K. Tian, Effective adsorption and removal of Cr (VI) from wastewater using magnetic composites prepared by synergistic effect of polypyrrole and covalent organic frameworks, *Sep. Purif. Technol.*, 2024, **336**, 126222, DOI: 10.1016/j.seppur.2023.126222.

15 L. Zhang, W. Niu, J. Sun and Q. Zhou, Efficient removal of Cr(VI) from water by the uniform fiber ball loaded with polypyrrole: Static adsorption, dynamic adsorption and mechanism studies, *Chemosphere*, 2020, **248**, 126102, DOI: 10.1016/j.chemosphere.2020.126102.

16 S. M. Anush and B. Vishalakshi, Modified chitosan gel incorporated with magnetic nanoparticle for removal of Cu (II) and Cr (VI) from aqueous solution, *Int. J. Biol. Macromol.*, 2019, **133**, 1051–1062, DOI: 10.1016/j.ijbiomac.2019.04.179.

17 C. Fan, K. Li, Y. He, Y. Wang, X. Qian and J. Jia, Evaluation of magnetic chitosan beads for adsorption of heavy metal ions, *Sci. Total Environ.*, 2018, **627**, 1396–1403, DOI: 10.1016/j.scitotenv.2018.02.033.

18 P. S. Bakshi, D. Selvakumar, K. Kadirvelu and N. S. Kumar, Chitosan as an environment friendly biomaterial - a review on recent modifications and applications, *Int. J. Biol. Macromol.*, 2020, **150**, 1072–1083, DOI: 10.1016/j.ijbiomac.2019.10.113.

19 M. Jafarnejad, M. D. Asli, F. A. Taromi and M. Manoochehri, Synthesis of multi-functionalized Fe_3O_4-NH_2-SH nanofiber based on chitosan for single and simultaneous adsorption of Pb(II) and Ni(II) from aqueous system, *Int. J. Biol. Macromol.*, 2020, **148**, 201–217, DOI: 10.1016/j.ijbiomac.2020.01.017.

20 C. Zheng, H. Zheng, Y. Wang, Y. Wang, W. Qu, Q. An and Y. Liu, Synthesis of novel modified magnetic chitosan particles and their adsorption performance toward Cr (VI), *Bioresour. Technol.*, 2018, **267**, 1–8, DOI: 10.1016/j.biortech.2018.06.113.

21 Y. Shi, J. Feng, Z. Zhang, N. Cao, J. Li, H. Li, L. Li, Q. Hua, Q. Ma and K. Zhang, Simultaneous removal of Cr (VI) anions and metal cations by EDTA-crosslinking-chitosan/polypyrrole composites, *Sep. Purif. Technol.*, 2023, **327**, 124926, DOI: 10.1016/j.seppur.2023.124926.

22 Y. Liu, H. Zhou, J. Wang, D. Yu, Z. Li and R. Liu, Facile synthesis of silver nanocatalyst decorated Fe_3O_4@PDA core-shell nanoparticles with enhanced catalytic properties and selectivity, *RSC Adv.*, 2022, **12**(7), 3847–3855, DOI: 10.1039/d1ra09187e.

23 H. Wang, X. Yuan, Y. Wu, X. Chen, L. Leng, H. Wang, H. Li and G. Zeng, Facile synthesis of polypyrrole decorated reduced graphene oxide-Fe_3O_4 magnetic composites and its application for the Cr(VI) removal, *Chem. Eng. J.*, 2015, **262**, 597–606, DOI: 10.1016/j.cej.2014.10.020.

24 L. Seid, D. Lakhdari, M. Berkani, O. Belgherbi, D. Chouder, Y. Vasseghian and N. Lakhdari, High-efficiency electrochemical degradation of phenol in aqueous solutions using Ni-PPy and Cu-PPy composite materials, *J. Hazard. Mater.*, 2022, **423**, 126986, DOI: 10.1016/j.jhazmat.2021.126986.

25 Z. A. Sutirman, E. A. Rahim, M. M. Sanagi, K. J. Abd Karim and W. A. Wan Ibrahim, New efficient chitosan derivative for Cu (II) ions removal: Characterization and adsorption performance, *Int. J. Biol. Macromol.*, 2020, **153**, 513–522, DOI: 10.1016/j.ijbiomac.2020.03.015.

26 X. Peng, W. Zhang, L. Gai, H. Jiang, Y. Wang and L. Zhao, Dedoped Fe_3O_4/PPy nanocomposite with high anti-interfering ability for effective separation of Ag(I) from mixed metal-ion solution, *Chem. Eng. J.*, 2015, **280**, 197–205, DOI: 10.1016/j.cej.2015.05.118.

27 Y. Li, J. Sun, Q. Du, L. Zhang, X. Yang, S. Wu, Y. Xia, Z. Wang, L. Xia and A. Cao, Mechanical and dye adsorption properties of graphene oxide/chitosan composite fibers prepared by wet spinning, *Carbohydr. Polym.*, 2014, **102**, 755–761, DOI: 10.1016/j.carbpol.2013.10.094.

28 R. A. Latour, The Langmuir isotherm: A commonly applied but misleading approach for the analysis of protein adsorption behavior, *J. Biomed. Mater. Res. A*, 2014, **103**(3), 949–958, DOI: 10.1002/jbm.a.35235.

29 G. Z. Kyzas, P. I. Siafaka, E. G. Pavlidou, K. J. Chrissafis and D. N. Bikiaris, Synthesis and adsorption application of succinyl-grafted chitosan for the simultaneous removal of zinc and cationic dye from binary hazardous mixtures, *Chem. Eng. J.*, 2015, **259**, 438–448, DOI: 10.1016/j.cej.2014.08.019.

30 S. Hao, Q. Zhang, Y. Wang, W. Zhang and J. Huang, Preparation and adsorption properties of green sustainable biomass carbon microspheres, *Ind. Eng. Chem. Res.*, 2022, **61**(30), 11249–11261, DOI: 10.1021/acs.iecr.2c00094.

31 U. Maheshwari, B. Mathesan and S. Gupta, Efficient adsorbent for simultaneous removal of Cu(II), Zn(II) and Cr (VI): Kinetic, thermodynamics and mass transfer mechanism, *Process Saf. Environ. Prot.*, 2015, **98**, 198–210, DOI: 10.1016/j.psep.2015.07.010.

32 R. Saadi, Z. Saadi, R. Fazaeli and N. E. Fard, Monolayer and multilayer adsorption isotherm models for sorption from aqueous media, *Korean J. Chem. Eng.*, 2015, **32**(5), 787–799, DOI: 10.1007/s11814-015-0053-7.

33 S. Çınar, Ü. H. Kaynar, T. Aydemir, S. Çam Kaynar and M. Ayvacıklı, An efficient removal of RB5 from aqueous solution by adsorption onto nano-ZnO/Chitosan composite beads, *Int. J. Biol. Macromol.*, 2017, **96**, 459–465, DOI: 10.1016/j.ijbiomac.2016.12.021.

34 R. Das, M. Bhaumik, S. Giri and A. Maity, Sonocatalytic rapid degradation of Congo red dye from aqueous solution using magnetic Fe^0/polyaniline nanofibers, *Ultrason. Sonochem.*, 2017, **37**, 600–613, DOI: 10.1016/j.ultsonch.2017.02.022.

35 L. Du, P. Gao, Y. Liu, T. Minami and C. Yu, Removal of Cr (VI) from aqueous solution by polypyrrole/hollow mesoporous silica particles, *Nanomaterials*, 2020, **10**(4), 686, DOI: 10.3390/nano10040686.

36 L. Du, P. Gao, Y. Meng, Y. Liu, S. Le and C. Yu, Highly efficient removal of Cr (VI) from aqueous solutions by polypyrrole/monodisperse latex spheres, *ACS Omega*, 2020, **5**(12), 6651–6660, DOI: 10.1021/acsomega.9b04438.

37 N. Wang, J. Chen, J. Wang, J. Feng and W. Yan, Removal of methylene blue by Polyaniline/TiO_2 hydrate: Adsorption

kinetic, isotherm and mechanism studies, *Powder Technol.*, 2019, **347**, 93–102, DOI: **10.1016/j.powtec.2019.02.049**.

38 W. Fang, X. Jiang, H. Luo and J. Geng, Synthesis of graphene/SiO_2@polypyrrole nanocomposites and their application for Cr(VI) removal in aqueous solution, *Chemosphere*, 2018, **197**, 594–602, DOI: **10.1016/j.chemosphere.2017.12.163**.

39 S. Deng and R. Bai, Removal of trivalent and hexavalent chromium with aminated polyacrylonitrile fibers: performance and mechanisms, *Water Res.*, 2004, **38**(9), 2424–2432, DOI: **10.1016/j.watres.2004.02.024**.

40 Y. Xu, J. Chen, R. Chen, P. Yu, S. Guo and X. Wang, Adsorption and reduction of chromium (VI) from aqueous solution using polypyrrole/calcium rectorite composite adsorbent, *Water Res.*, 2019, **160**, 148–157, DOI: **10.1016/j.watres.2019.05.055**.